Bulletin of the Seismological Society of America, Vol. 86, No. 2, pp. 306–319, April 1996

Horizontal-to-Vertical Spectral Ratio and Geological Conditions: The Case of Garner Valley Downhole Array in Southern California

by N. Theodulidis, P.-Y. Bard, R. Archuleta, and M. Bouchon

Abstract The aim of the present article is to further check the use of the horizontal-to-vertical (h/v) spectral ratio, which has been recently suggested as an indicator of site effects. The data set consists of 110, three-component, high sensitivity accelerograms, recorded at five different depths by the Garner Valley Downhole Array (GVDA), in southern California, with peak ground accelerations $0.0002\ g \leqq a_g \leqq 0.04\ g$, magnitudes $3.0 \leqq M_L \leqq 4.6$, and hypocentral distances $16\ \text{km} \leqq R \leqq 107\ \text{km}$. First, the stability of the (h/v) spectral ratio is investigated by computing the mean for the whole data set in different depths. The (h/v) spectral ratio on the surface is compared with the surface-to-depth standard spectral ratio, with theoretical *S*-wave transfer functions derived from the vertical geotechnical profile, as well as with the (h/v) spectral ratio of synthetic accelerograms generated by the discrete wavenumber method. Both theoretical and experimental data show a good stability of the (h/v) spectral ratio shape, which is in good agreement with the local geological structure and is insensitive to the source location and mechanism. However, the absolute level of the (h/v) spectral ratio depends on the wave field and is different from the surface-to-depth spectral ratio. Consequently the (h/v) spectral ratio technique provides only partially the information that can be obtained from a downhole array. But surface-to-depth ratios may also be misleading because they combine effects at surface and at depth.

Introduction

The importance of local site geology in seismic design is nowadays well established. The evaluation of site effects on strong ground motion has been extensively studied during the last two decades and is thoroughly reviewed by Aki (1988, 1993) and Finn (1991). The most standard method for characterizing site amplification is the spectral ratio technique. It requires a pair of instruments, one located at the site under investigation (generally on alluvium) and the other on a "reference site," preferably a nearby rock site; both instruments must simultaneously record the ground motion of a number of events. In many cases, it is difficult to find sites on bedrock that are close enough to alluvium ones. In addition, outcrops of bedrock sites are usually weathered, and the resulting superficial velocity gradient is capable of influencing the "reference" ground motion. In order to overcome these shortcomings, downhole arrays whose recordings allow for a direct comparison of the response of the superficial layers to the response of the underlying bedrock have been developed. Data obtained from these arrays put some light into the efficiency of theoretical models used (Seed and Idriss, 1970; Joyner *et al.,* 1976; Redpath and Lee, 1986) and into the interference between incident and reflected wave field (Shearer and Orcutt, 1987; Blakeslee and Malin, 1991; Aster and Shearer, 1991) as well as into the near-surface attenuation or amplification (Hauksson *et al.,* 1987; Malin *et al.,* 1988; Seale and Archuleta, 1989; Liu *et al.,* 1992).

Apart from the standard spectral ratio technique, recently, another nonreference site-dependent technique was introduced by Nakamura (1989) for the evaluation of site effects. This technique, originally applied to microtremors (Ochmachi *et al.,* 1991; Field and Jacob, 1993; Field *et al.,* 1993; Lachet and Bard, 1994), has also been applied to weak- (Lermo and Chavez-Garcia, 1993; Duval, 1994; Field, 1994) and, in some cases, to strong-motion studies (Lermo and Chavez-Garcia, 1993; Theodulidis and Bard, 1995). This technique, which is comparable with the so-called receiver-function technique, applied to studies of the upper mantle and crust from teleseismic records (Langston, 1979), assumes that the local site conditions do not significantly influence the vertical component of the ground motion.

The Garner Valley Downhole Array (GVDA) has been in full operation since the summer of 1989 and consists of 5 three-component accelerometers placed at depths of 0, 6, 15, 22, and 220 m. Archuleta *et al.* (1992, 1993), after a preliminary data analysis, observed for the frequency range

of 1.7 to 30 Hz a mean spectral amplification of approximately 10 between the surface and a depth of 220 m, with clear resonance peaks at 1.7, 3.0, and 12.0 Hz. Using only the GVDA data with peak ground accelerations $a_g < 0.1\ g$, Mohammadioun *et al.* (1992) concluded that the surface-to-depth spectral ratios remain relatively stable despite the fact that they come from various magnitudes and distances. In addition, they showed that a simple 1D model without provisions for nonlinear behavior can satisfactorily explain the observed average transfer functions. Gariel *et al.* (1993) calculated observed transfer functions for over 200 events and compared them with theoretical ones relying on a 1D model. They found a good agreement between observed and theoretical transfer functions and concluded that the influence of interface geometry was not important. They also showed, based on records from the Palm Springs earthquake (M = 6.1, R = 45 km) with maximum peak ground acceleration $a_g = 0.1\ g$, that there is no indication of nonlinear behavior of the sediment deposits. Pecker and Mohammadioun (1993) using 218 events recorded at the Garner Valley downhole array evaluated the mean transfer functions between different pairs of stations down to 22 m and proposed some corrections to the elastic properties of the geotechnical profile of the array. Coutant (1995), using data from the Garner Valley downhole array, showed that shallow S-wave anisotropy significantly affects the earthquake records at the surface in the frequency range from 1 to 30 Hz.

In this study, 110 three-component accelerograms from the GVDA are selected for an estimation of the significant site-effect factors obtained when using both the standard spectral ratio and the (h/v) spectral ratio technique. The results from these two methods are compared. For four selected events, synthetic accelerograms are generated by applying the discrete wavenumber method, and the corresponding surface/depth spectral ratios as well as the (h/v) spectral ratios are compared with the instrumental observations. These results allow a careful discussion on the ability of the (h/v) spectral ratio technique to actually measure site effects.

Data Used

The Garner Valley Downhole Array (GVDA) in southern California is a five-element array of three-component, dual-gain force balance accelerometers that are capable of measuring accelerations from $3 \times 10^{-6}\ g$ to $2.0\ g$ over a frequency range from 0 to 100 Hz. Its location is close to the San Jacinto fault and is shown in Figure 1 along with the location of the 22 events used in this study. There is one surface and four downhole accelerometers placed at depths of 6, 15, 22, and 220 m within a 3- × 3-m area (Fig. 2). A more detailed presentation of the array configuration and instrument characteristics can be found in Archuleta *et al.* (1992, 1993).

The data set used in this study consists of 110 three-component accelerograms triggered by 22 events during the first year of the array operation, July 1989 through June 1990, with magnitudes $3.0 \leqq M_L \leqq 4.6$ and hypocentral distances 16 km $\leqq R \leqq$ 107 km (Archuleta *et al.*, 1992, 1993). The corresponding earthquake parameters are listed in Table 1. The accelerograms used have been recorded by the high-gain channels that have a flat amplitude response to acceleration between 0.025 and 100 Hz and a maximum acceleration capability of 0.1 g. The low-frequency limit of 0.025 Hz is not a concern, since small earthquakes recorded on the high-gain channel do not have durations that exceed

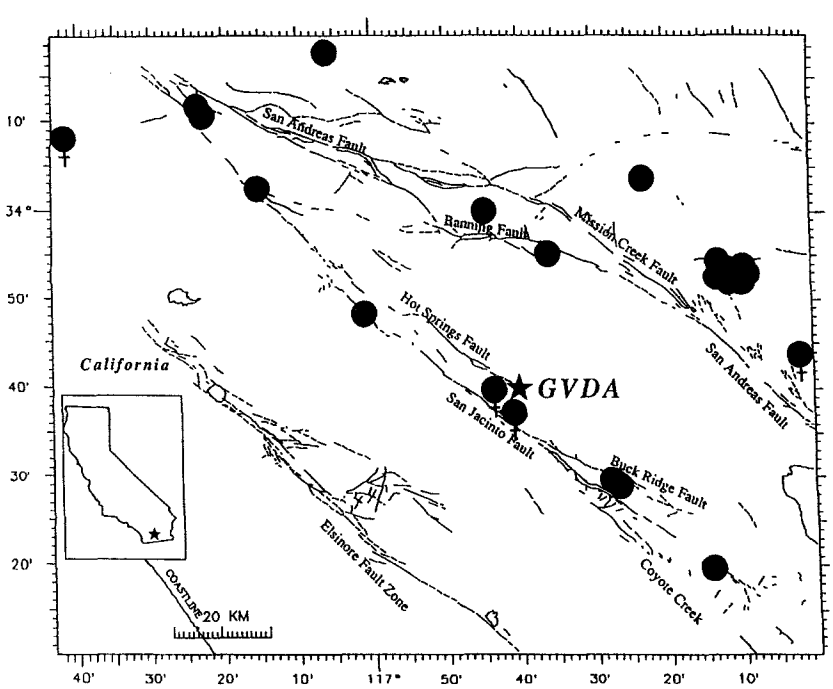

Figure 1. Map view of the region around GVDA (star) and the epicenters (full circles) of the 22 earthquakes used in this study, which have been recorded by the array from July 1989 to June 1990. Synthetic accelerograms were generated for the events indicated by a cross.

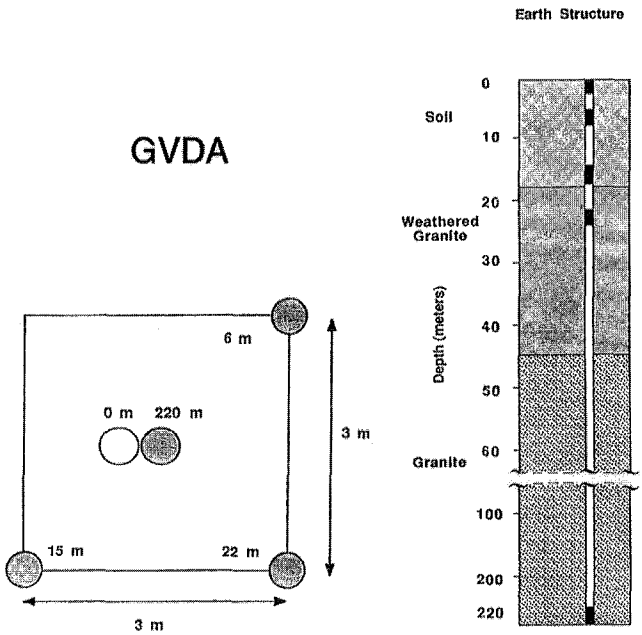

Figure 2. Plan view of the arrangement of the boreholes (shaded disks), the depth at which the accelerometer package is placed, and the earth structure at GVDA.

40 sec. The accelerograms were low-pass filtered at 30 Hz before use since, for the purpose of our study, the energy included in strong ground motion at higher frequencies can be considered as negligible. The peak ground accelerations of the filtered accelerograms range between 0.0002 and 0.04 g. The recordings with the highest peak ground acceleration, around 40 cm/sec^2 at the surface, are presented in Figure 3, where a surface-layer amplification factor, between 220 and 0 m, of about 5 is very clear.

The density, the velocity structure, and the quality factors beneath the GVDA are presented in Table 2. This information was taken from Pecker and Mohammadioun (1993) for depth range 0 to 45 m, from Archuleta *et al.* (1992, 1993) for depths 45 to 3000 m, and from Hough and Anderson (1988) for deeper layers. In fact, for depths greater than 22 m, the quality factor values, Qs, were calculated by the relation $1/Qs = 0.019/f$, considering $f \approx 10$ Hz, while Qp values were calculated by the relation $Qs/Qp \approx 1.2$ that was proposed for the study region by Hough and Anderson (1988).

Horizontal-to-Vertical and Standard Spectral Ratio Techniques

The standard spectral ratio technique, hereafter referred to as spectral ratio, that utilizes the horizontal Fourier amplitude motion recorded on an alluvium site, S_{HS}, to that recorded on the surface of a nearby rock site, S_{HB}, has been widely applied for site-effects evaluation. In this technique, the intense S-wave part of the record is mainly used for the estimation of the spectral ratio, S_T,

$$S_T = S_{HS}/S_{HB}. \tag{1}$$

The (h/v) spectral ratio technique, hereafter referred to as the (h/v) ratio, has been originally used to interpret site amplification conducted by microtremor measurements (Nakamura, 1989). Nakamura assumed that the vertical motion is not significantly amplified by the surface layers, with the exception of Rayleigh waves. Thus, denoting by S_{VS} and S_{VB} the vertical motion at the surface and at the bedrock in a certain depth, respectively, the ratio

$$E_T = S_{VS}/S_{VB} \tag{2}$$

should take values larger than unity with increasing effects of Rayleigh waves. If there are no Rayleigh waves, the value of this ratio should be close to unity. Making the further assumption that the effect of Rayleigh waves is about equal for vertical and horizontal components, the ratio S_T/E_T is considered to be a more reliable transfer function than S_T. It may be written

$$S_{TT} = S_T/E_T = (S_{HS}/S_{VS})/(S_{HB}/S_{VB}). \tag{3}$$

Then, based on microtremor observations at three sites, Nakamura assumes that the S_{HB}/S_{VB} ratio at a certain depth takes values around 1 for a wide frequency range so that the ratio $S_{TT} = S_{HS}/S_{VS}$ is, according to him, representative of the amplification factor of body waves.

In the present work, the entire accelerogram consisting of body waves, surface waves, multiply reflected waves, and scattered coda waves is considered. The main reasons for using the entire record length instead of separating the intense S-wave part of the motion are that first, in structural response evaluation for seismic excitation, the entire accelerogram is usually used, and second, the separation of a particular type of wave from the record is not a straightforward task because of scattering effects that affect all parts of the signal, except the very onset of P waves.

In order to provide more readable spectral ratios, the Fourier spectra of the accelerograms were smoothed by a triangular moving window having a 0.5-Hz half-width. Then, using the 5-sec noise of the pre-event memory for every individual horizontal and vertical component, the Fourier amplitude spectra of the signal and noise were compared for the frequency range 0.2 to 30 Hz. The spectral values of the signal were considered as meaningful only where the corresponding signal-to-noise ratio exceeded 3. For all frequencies where this criterion was not fulfilled, the spectral ratio or (h/v) ratio was not estimated. In estimating spectral ratios and (h/v) ratios, each horizontal component was independently used.

Applying the aforementioned methodology, it was found that, for all accelerograms recorded at the surface and

Table 1
Earthquake Parameters of the Accelerograms Used

No	Origin Time (y/m/d h:m:s)	M_L	Lat. (°N)	Long. (°W)	Distance Epic. (km)	Depth (km)	Azimuth (deg from N)
1	89/08/30 18:39:08	3.1	33 55.55	116 36.22	26.6	12.5	15.9
2	89/09/02 05:39:35	3.2	33 30.47	116 26.67	29.3	9.3	129.4
3	89/09/04 17:53:41	3.2	33 19.96	116 14.30	56.7	10.3	129.9
4	89/11/12 17:13:31	3.0	34 00.15	116 44.55	35.0	14.1	346.8
5	89/12/02 23:16:47	4.2	33 38.74	116 44.50	6.2	14.5	251.4
6	89/12/06 19:15:23	3.4	33 48.42	117 02.13	36.0	15.3	287.3
7	89/12/18 06:27:04	4.0	33 44.03	116 01.43	59.9	9.9	86.4
8	89/12/22 03:03:25	3.4	33 37.44	116 41.27	7.9	14.1	194.4
9	89/12/28 09:41:08	4.3	34 11.54	117 23.18	86.2	14.6	304.9
10	89/12/28 10:00:44	3.3	34 11.21	117 22.97	85.6	14.3	304.7
11	90/02/09 17:39:03	3.0	33 30.24	116 27.02	29.2	9.6	130.8
12	90/03/02 17:26:25	4.6	34 08.70	117 41.68	107.0	5.6	293.8
13	90/04/04 02:13:39	3.7	34 19.55	117 05.31	80.2	5.5	326.5
14	90/04/04 23:47:44	3.2	33 51.71	116 11.71	47.7	5.4	70.5
15	90/04/07 01:07:05	3.8	33 52.25	116 09.38	51.4	4.7	70.9
16	90/04/12 01:12:55	3.3	33 52.84	116 09.22	52.0	4.2	70.1
17	90/04/12 02:45:56	3.1	33 52.80	116 08.98	52.3	2.0	70.3
18	90/04/14 11:14:11	3.3	33 52.37	116 09.59	51.2	4.6	70.6
19	90/04/18 14:32:49	3.6	33 52.64	116 09.91	50.9	4.7	70.0
20	90/04/23 09:30:16	3.0	34 03.76	116 23.43	48.5	3.5	37.1
21	90/04/24 11:27:19	3.3	33 52.75	116 09.54	51.5	4.5	70.0
22	90/06/17 06:08:05	3.7	34 02.79	117 15.25	66.7	15.0	301.2

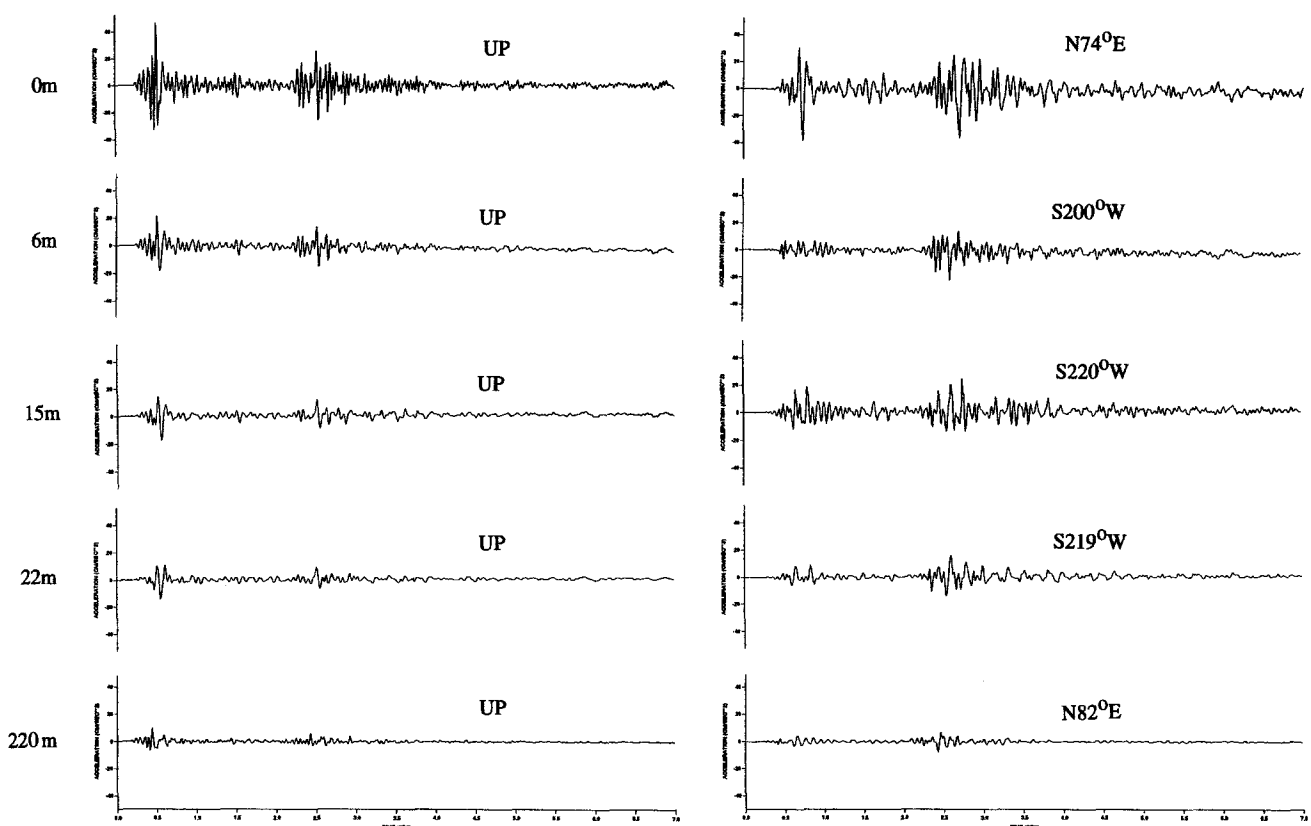

Figure 3. Horizontal and vertical components recorded at different depths and on the surface of the GVDA, during the event with magnitude $M_L = 4.2$, hypocentral distance $R = 16$ km (Table 1, number 5).

Table 2
Geotechnical Profile and Elastic Properties beneath Garner Valley Downhole Array

Depth (m)	ρ (g/cm^3)	V_p (m/sec)	V_s (m/sec)	Qp	Qs
0–1	1.95	400	90	14	17
1–2	1.95	400	130	14	17
2–4	2.00	400	165	14	17
4–6	2.00	400	190	14	17
6–8	2.00	2030	215	11	13
8–11.5	2.00	2030	240	11	13
11.5–15	2.00	2030	260	11	13
15–18	2.05	2030	285	42	50
18–22	2.20	2030	450	42	50
22–45	2.40	2030	1100	210	250
45–150	2.80	2460	1310	420	500
150–3000	2.80	5500	2500	420	500
3000–5000	2.80	5800	3400	420	500
>5000	2.80	6000	3500	420	500

for frequencies less than about 0.4 Hz, the signal-to-noise ratio is less than 3. For the 6-m depth, this lower-frequency limit was also observed at about 0.4 Hz, whereas for 15, 22, and 220 m, it ranges between 0.2 and 0.4 Hz. For comparison reasons, the frequency range 0.35 to 20 Hz was adopted in all relevant figures. For every discrete frequency, the mean and mean ± 1 standard deviation of the logarithmic values of the (h/v) ratio or spectral ratio were calculated.

Figure 4 displays the mean and mean $+1$ standard deviation of the (h/v) ratio, for the five depth levels of the GVDA. The -1 standard deviation is not shown in order to simplify the plots since its values are symmetric to the $+1$ standard deviation with respect to the mean curve. The stability of these ratios, as deduced from the standard deviation values, at each individual depth is remarkable, while their shape drastically changes from the surface to 220 m, indicating the influence of depth and site geology. A prominent peak around 1.8 Hz for the upper four stations, with decreasing amplitude from surface to depth, is observed, while for the one installed at a depth of 220 m, a trough clearly appears. For frequencies higher than about 3 Hz and for the upper four stations, the increase of the number of troughs with increasing depth is observed, which is consistent with interferences between the incident and reflected wave field. It is also evident that the (h/v) ratio at a depth of 220 m, for frequencies less than about 10 Hz, is not far from unity, at least within a factor of 2, which is a typical uncertainty level when dealing with spectral ratios (Tucker and King, 1984; Tucker *et al.*, 1984). Thus, Nakamura's hypothesis that the ratio S_{HB}/S_{VB} takes values around unity, made for microtremor measurements, is also verified in the case of strong ground motion, at least for the aforementioned frequency range and at large depths only. The drastic change of the (h/v) ratio observed at a depth of 220 m in the frequency range 10 to 12 Hz is difficult to explain. One possibility is that a cultural feature of some sort may affect actual signal at this frequency range. However, a cultural source is not yet proven, and this drastic change should be viewed with caution.

By applying the spectral ratio technique and considering as reference station the one at the 220-m depth, the empirical transfer functions, 0 m/220 m, for the 22 events of Table 1 were calculated. The corresponding mean and mean $+1$ standard deviation of the spectral ratio is shown in Figure 5 along with the mean and mean $+1$ standard deviation of the (h/v) ratio at surface. The spectral ratio stability, as deduced from the standard deviation values, is comparable with that of the mean (h/v) ratio on the surface. In Figure 6, the standard deviation obtained by either method as a function of frequency is shown. The values of the standard deviation range from about 1.2 to 1.8, with an exception at frequencies lower than 0.5 Hz, where it reaches up to 2.5. Both standard deviations are comparable, except for frequencies around 3 and 12 Hz, where the spectral ratio gives higher values. Comparing the mean spectral ratio with the mean (h/v) ratio on the surface (Fig. 5), a similarity in shape is evident for frequencies less than 10 Hz and greater than 13 Hz. The trough observed in spectral ratio for frequencies 10 to 12 Hz is not apparent in (h/v) ratio. More specifically, for the spectral ratio, peaks clearly appear at about 1.8, 3.0, 6, 8, and 13 Hz, with amplification values fluctuating from about 7 to 14. The (h/v) ratio exhibits a somewhat simpler shape with, however, clear peaks at similar frequencies: 1.8, 6, and 8 Hz. The second peak at about 3 Hz and the last at 13 Hz almost disappear. For these two frequencies, as already mentioned, the standard deviations of the spectral ratio are higher than those of the (h/v) ratio. The corresponding mean amplification values range from about 2.5 to 3.5, while the spectral ratio for the same resonance frequencies gives amplification values 2 to 6 times greater than the (h/v) ratio. This large difference may be partially decreased if the spectral ratio is corrected for the fact that the reference bedrock site is at depth and not at surface. Assuming a free surface factor of 2, the spectral ratio amplitude obtained can be divided by this factor, and thus the difference is reduced. But in doing so, we assume that the incident wave field is mainly vertically propagating near the surface and that most of the surface-reflected energy is trapped and dissipated in the upper layers so that the seismic energy at a depth of 220 m is primarily in the incident wave field.

Theoretical H/V Ratio and Spectral Ratio for Incident *P* and *SV* Plane Waves

In order to interpret the aforementioned results, it was considered interesting to investigate the (h/v) ratio of body waves arriving at GVDA. For this purpose, a 1D code based on the reflectivity method (Kennett and Kerry, 1979) was used in order to compute the surface response to plane *P* and *SV* waves for various incidence angles. The velocity structure and the elastic properties considered were taken from Table 2. The horizontal, u, and vertical, w, components of the surface response to incident *P* and *SV* upgoing plane waves were

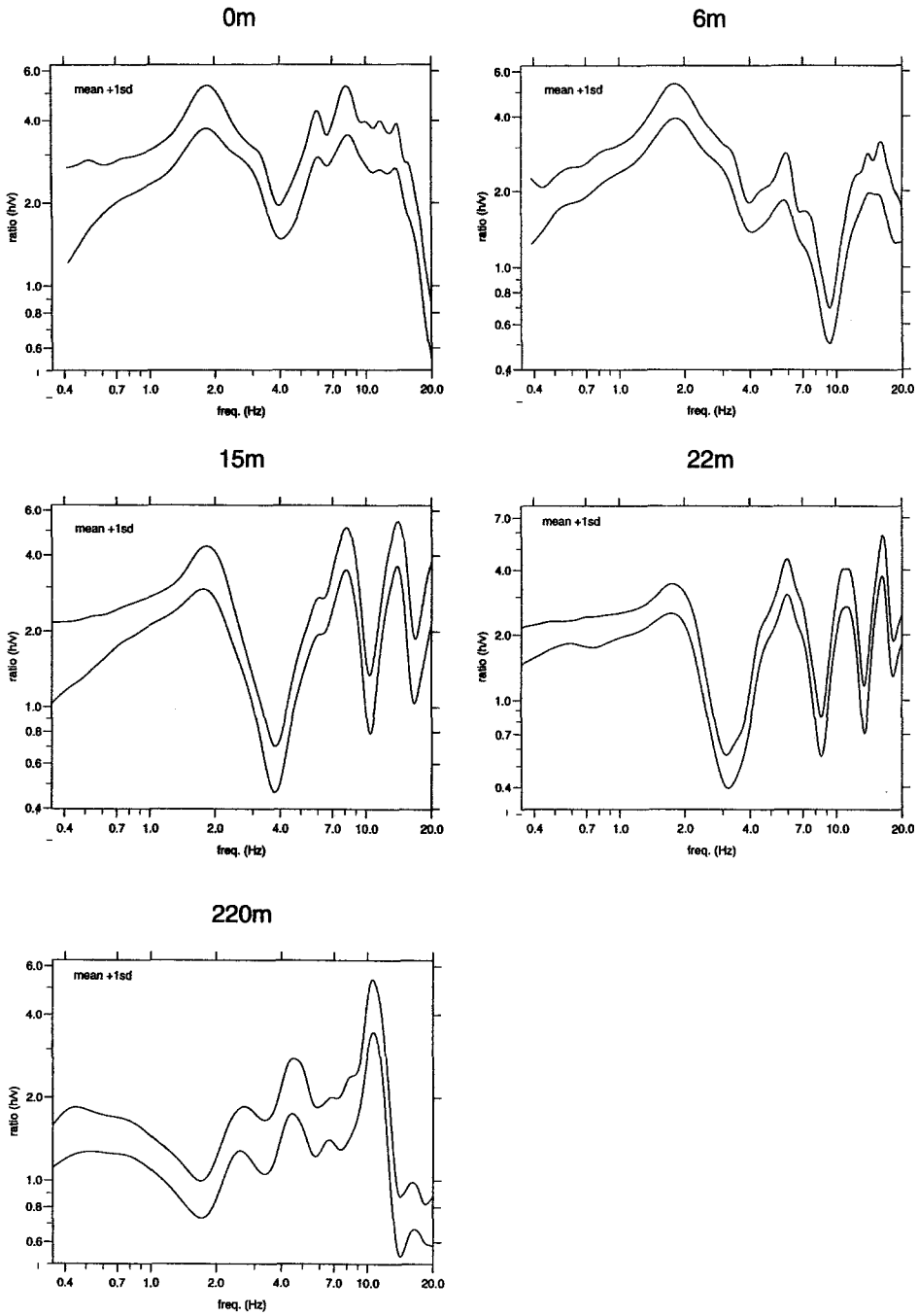

Figure 4. Mean and mean + 1 standard deviation of the (h/v) ratio based on the recordings of the 22 events, for different depths at GVDA.

separated and their (u/w) or equivalently (h/v) ratios were calculated. Results are shown in Figure 7 for various angles of incidence. The (h/v) ratio due to incident P and SV plane waves exhibit rather stable resonant "bumps" in the frequency range 2 to 4 Hz, 6.0 to 9.0 Hz, and around 14 Hz, whose positions are almost independent of the incidence angle, although their absolute amplitudes vary significantly.

It must be mentioned here that theoretically the very first onset of P arrivals is expected to have an incidence angle equal to 0°, resulting to an (h/v) ratio equal to zero. Using the onset of P-wave pulses of five recordings of the same event, the incidence angle for different depths of GVDA was investigated (Fig. 8). For this purpose, the nonfiltered recordings were used, and the radial component of the ground motion was calculated. The angle of incidence then was estimated and found to decrease from 16.9° at a depth of 220 m to 0° on the surface. This is what was expected for the very first onset of the direct P arrival. However, this is not valid for the rest of the signal since scattered waves from various directions randomly affect the angle of incidence.

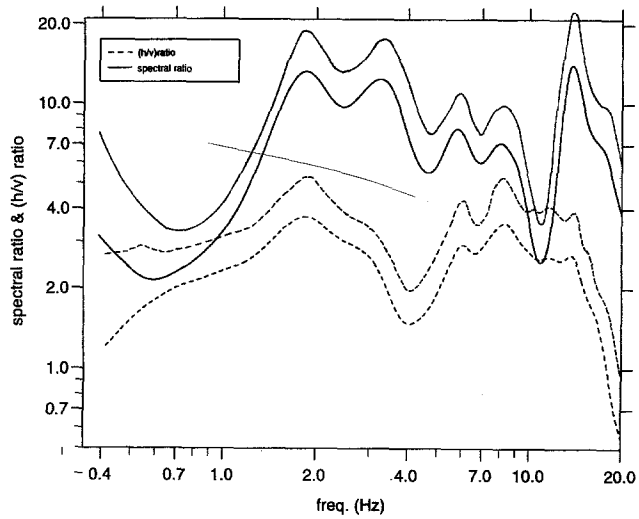

Figure 5. Comparison of the mean and mean +1 standard deviation (h/v) ratio with spectral ratio based on data recorded at the surface of GVDA (Table 1).

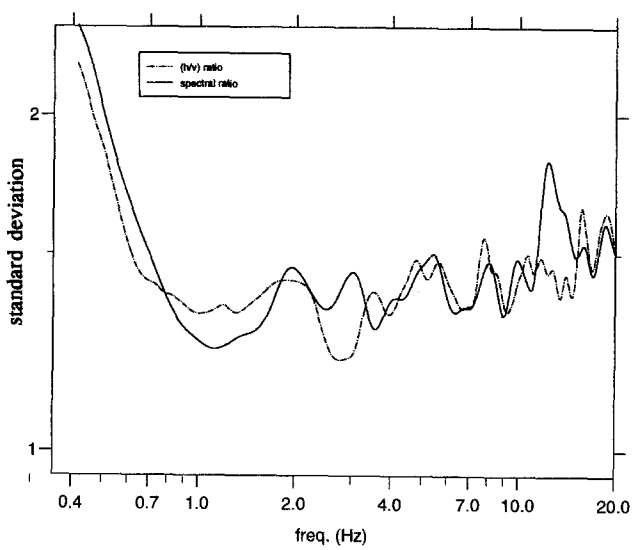

Figure 6. Standard deviation values of the observed (h/v) ratio and spectral ratio, as a function of frequency.

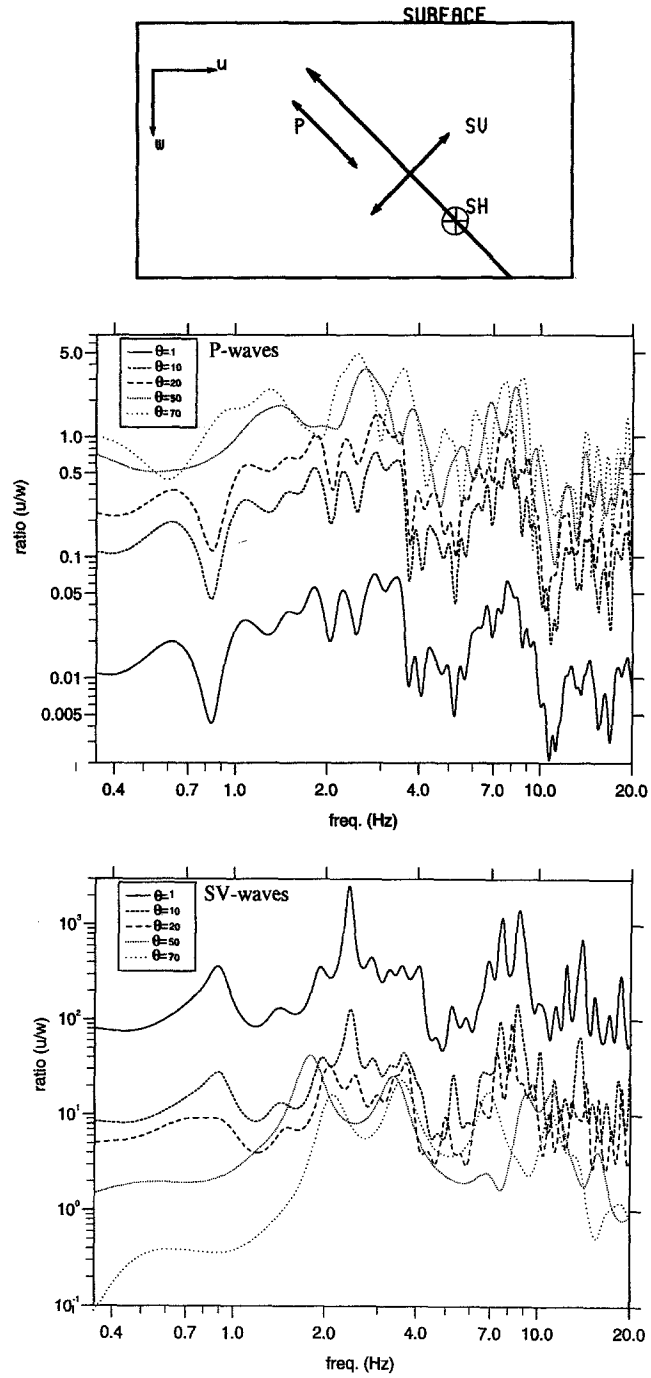

Figure 7. Theoretical (u/w) ratio due to the incidence of P or SV waves for various angles of incidence, θ, utilizing the vertical geotechnical profile of Table 2.

In Figure 9, the mean spectral ratio, based on data, at the surface of GVDA and the theoretically calculated 0 m/220 m S-wave transfer function for 0° incidence angle are compared. The mean spectral ratio, based on data, is not presented for frequencies less than 0.55 Hz, where as has been shown (Fig. 6), a drastic increase of the standard deviation values takes place. The shape of the two spectral ratios as well as their amplitudes are in good agreement: the relative "smoothness" of the observed ratio with respect to the theoretical one may be explained by the fact that observed data include direct and scattered waves with very different angles of incidence.

As can be deduced from Figure 9, the velocity model is quite representative of the observations. In turn, it means that we can compare the observed (h/v) ratios at different depths with the corresponding theoretical S-wave transfer functions, that is, the response at the surface, 6, 15, 22, and 220 m depths to incident SV upgoing plane waves with incidence angle equal to 0°. So, in Figure 10, comparing the (h/v) ratio, based on data, with the theoretical S-wave trans-

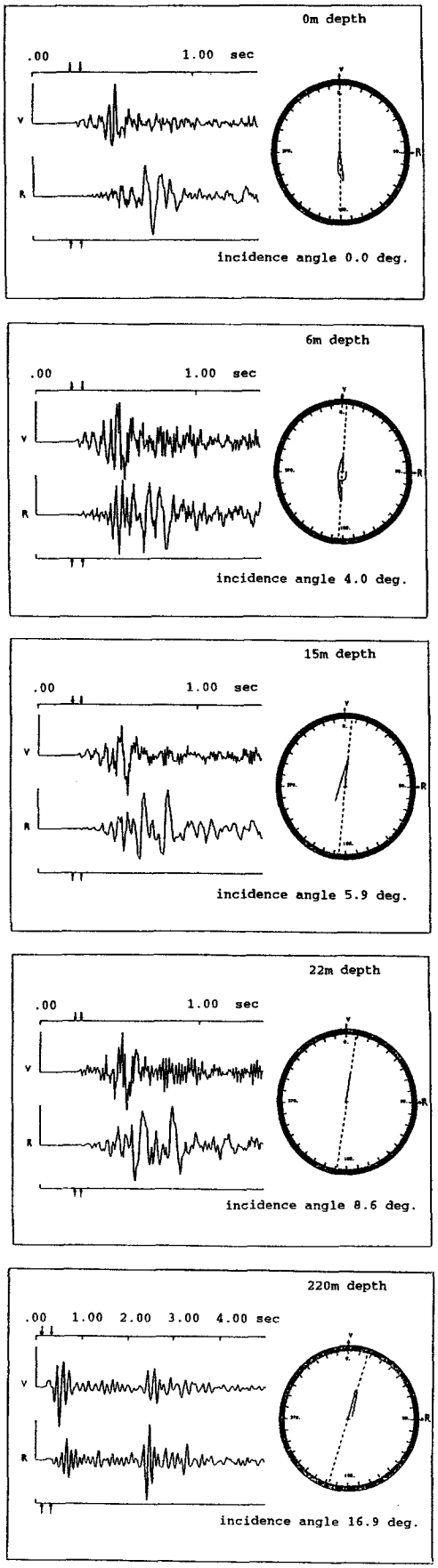

Figure 8. Diagrams showing variation of the incidence angle of the very first *P*-wave pulse at 220, 22, 15, 6, and 0 m depths at GVDA. The two arrows on the time scale define the time window used for each diagram (V vertical; R radial).

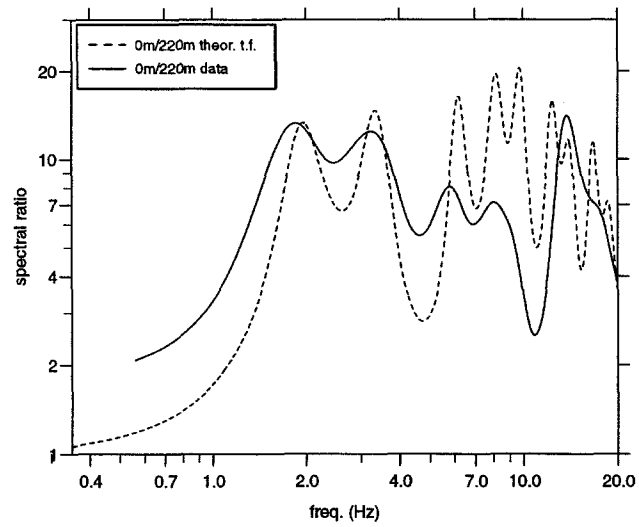

Figure 9. Comparison between the observed and theoretical spectral ratio at the surface of GVDA. For the latter, vertically incident *S* waves were considered.

fer function for different depths of the GVDA, a generally good agreement is obtained. More specifically, remarkable agreement is observed both in shape and in amplitude at depths of 22 and 15 m, while at a depth of 6 m and at the surface, the (h/v) ratio is slightly shifted to lower frequencies. At a depth of 220 m, a striking difference in amplitude is observed around 10 to 12 Hz, which is connected to the drastic change of the (h/v) ratio at this depth.

Since the theoretical *S*-wave transfer function seems to be in agreement with the (h/v) ratio, the idea of a normalized (h/v) ratio at the surface emerges. By dividing the observed (h/v) ratio at the surface by the (h/v) ratio at a depth of 220 m and comparing it with the observed spectral ratio at the surface, any influence of site effects on the vertical component may be indirectly seen. Thus, the normalized (h/v) ratio shape at the surface becomes very similar to the spectral ratio shape at the surface, for the whole frequency range (Fig. 11). Consequently, it becomes clear that the site geology practically does not affect the transfer function shape of the vertical component. In fact, the shape of the normalized (h/v) ratio, compared to (h/v) ratio at the surface (Fig. 5), has essentially changed in the frequency range between 10 and 13 Hz, where after the normalization, a trough appears similar to the one observed in the spectral ratio. But, as has been discussed before, the signal in this frequency range must be treated with caution.

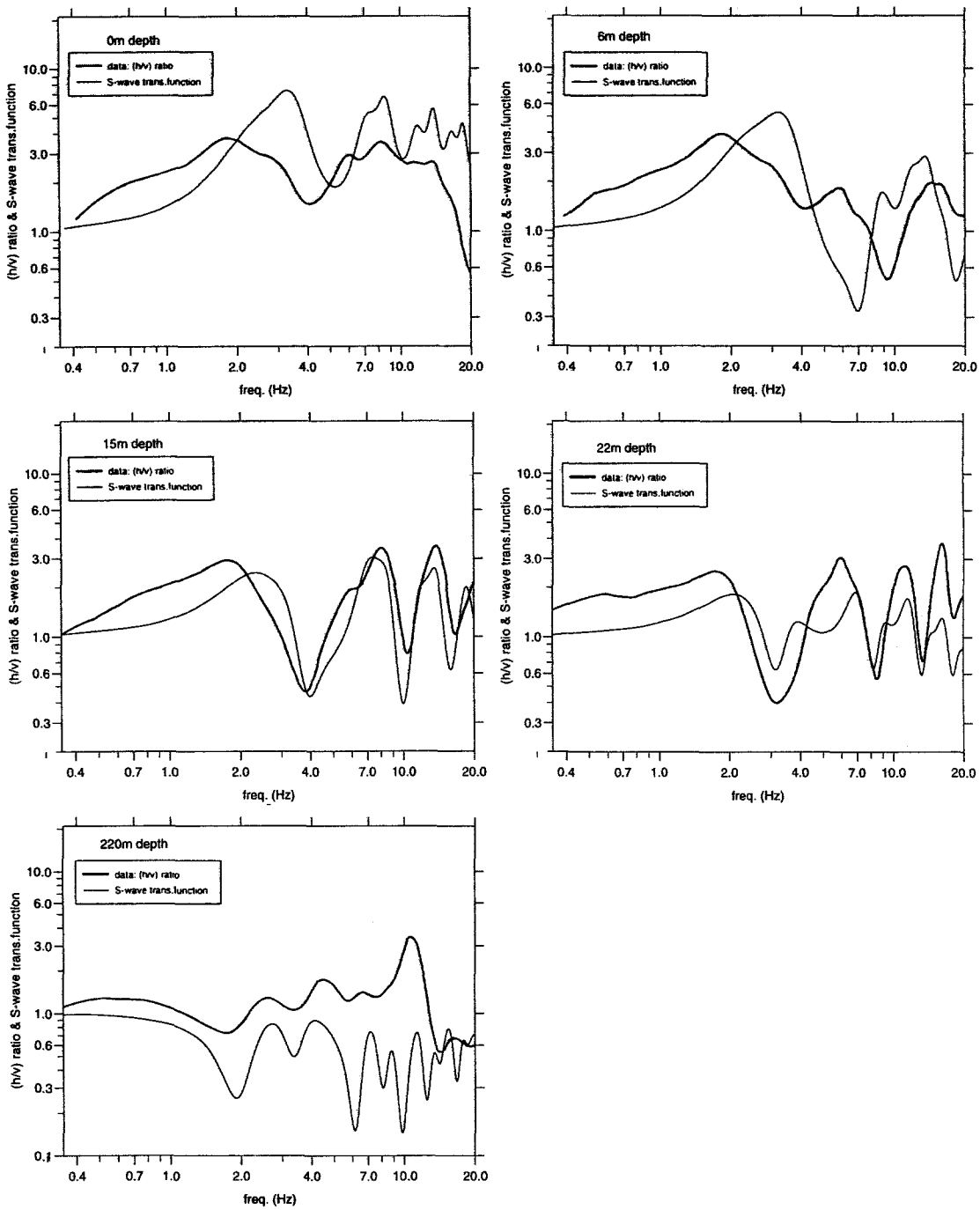

Figure 10. Comparison between the observed (h/v) ratio at GVDA and theoretical response of the surface as well as of different depths to incident *SV* upgoing plane waves vertically propagating.

(H/V) Ratio and Spectral Ratio from Synthetic Accelerograms Generated by the Discrete Wavenumber Method

Under the assumption that source mechanism, propagation path properties, and site conditions are known or may be realistically adopted, an *a posteriori* numerical simulation for four selected events of Table 1 was attempted. For the numerical simulation, the reflectivity code AXITRA was used (Coutant, 1989), which generates synthetic seismograms based on the discrete wavenumber (DWN) method (Bouchon, 1981). This code computes the Green's function in a horizontally stratified medium in the frequency domain for a double-couple point source and a given receiver. These Green's functions are then convolved with an appropriate

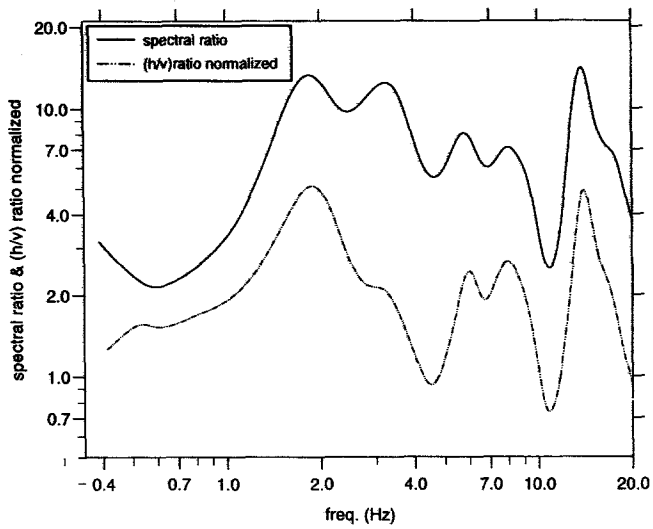

Figure 11. Comparison between the observed spectral ratio and normalized (h/v) ratio at the surface of GVDA. The latter resulted by dividing the (h/v) ratio at surface with the (h/v) ratio at a depth of 220 m.

source time function and a chosen source mechanism in order to obtain a time history.

The recordings chosen for the numerical simulation are the number 5, 7, 8, and 12 events, indicated by a cross in Figure 1, having pairs of magnitude-hypocentral distance (M_L = 4.2, R = 16 km), (M_L = 4.0, R = 61 km), (M_L = 3.4, R = 16 km), and (M_L = 4.6, R = 107 km), respectively. It is believed that this choice represents satisfactorily our data set, including different waveforms due to various source spectra at increasing hypocentral distances.

Since the focal mechanism was not known for the four aforementioned events, a fault with strike = 135°, dip = 90°, and rake = 45° was arbitrarily considered. As a source function, a trapezoid model was applied for all the events with a rise time ranging from about 0.05 to 0.1 sec and a source process time from about 0.05 to 0.2 sec. The moment, M_0, was calculated by the formula (Bakun and Lindh, 1977)

$$\log M_0 = 1.21M_L + 17.02 \qquad (4)$$

proposed for earthquakes near Oroville, California, for $0.1 < M_L < 5.7$.

In Figure 12, the synthetic accelerograms are compared with the recorded ones for event number 8 (M_L = 3.4, R = 16 km). The lack of scattered P and S waves is obvious in the synthetics. The (h/v) ratio and the spectral ratio were also calculated for the four aforementioned synthetic accelerograms, by applying for each component the same smoothing as in the case of the actual recordings. In Figures 13 and 14, comparisons are made between the (h/v) ratios and the spectral ratios, 0 m/220 m, of the observed and synthetic accelerograms. The following remarks are noteworthy. There is generally good agreement of the peak positions of spectral ratios and (h/v) ratios for both experimental and

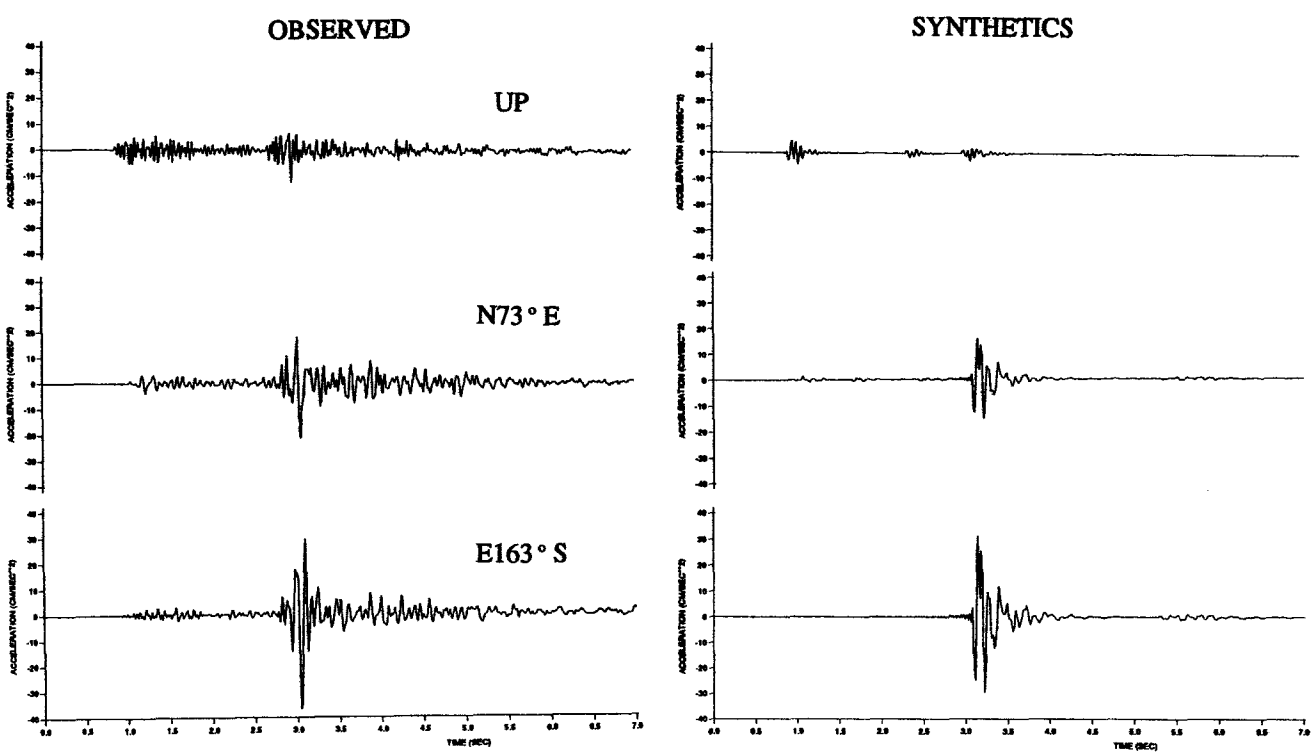

Figure 12. Comparison between the observed and synthetic accelerograms at the surface of GVDA for the event with M_L = 3.4, R = 16 km (Table 1, number 8).

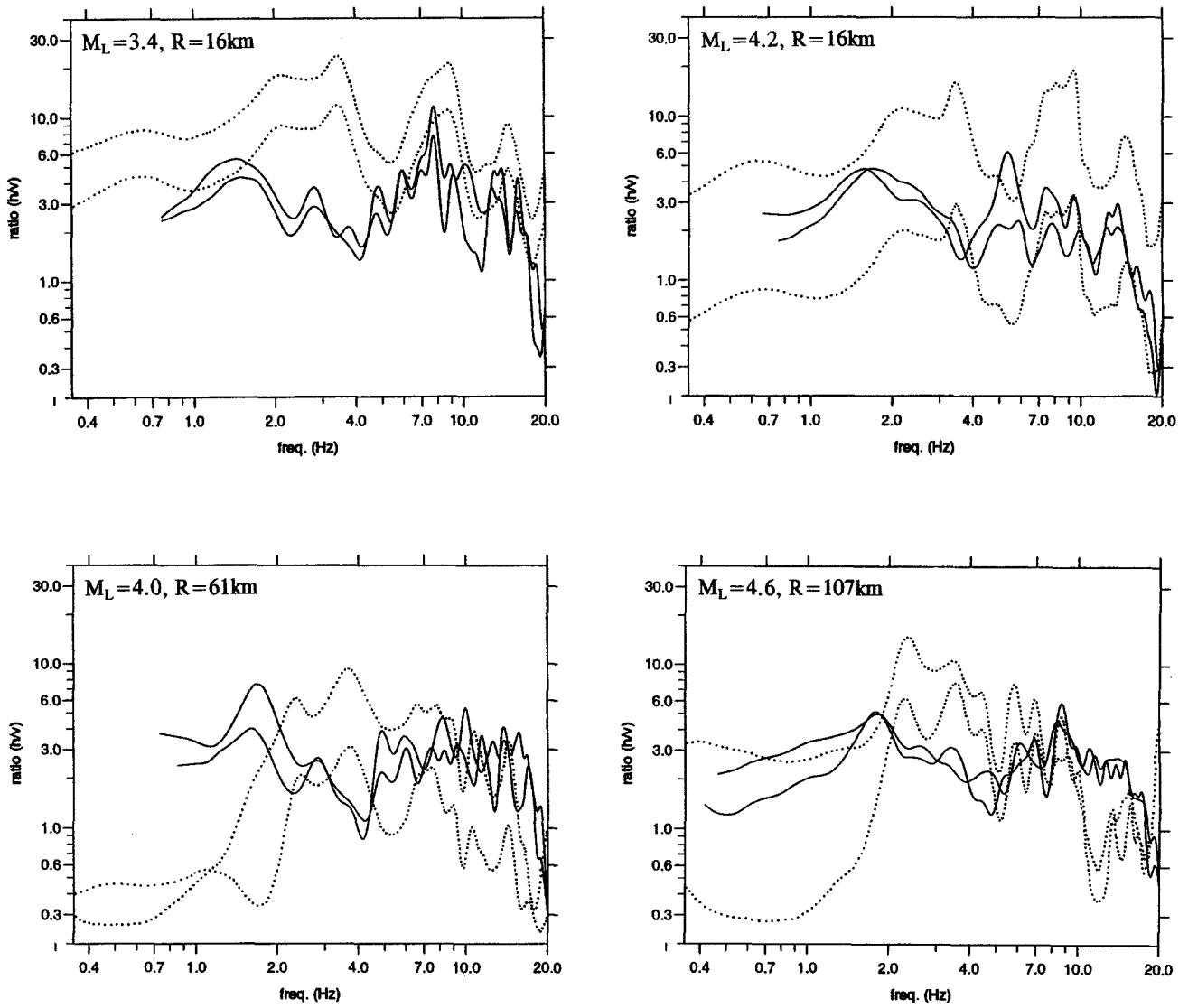

Figure 13. The (h/v) ratio (solid line) on the surface of GVDA for four selected recordings (Table 1, numbers 5, 7, 8, and 12), in comparison with those corresponding to the synthetic accelerograms generated by the discrete wavenumber method (dotted line).

synthetic ground motions. The spectral ratio of the synthetics shows a better agreement of the peaks position, and its amplitude is comparable with that of the experimental data, with an average amplification around 10 to 15 for all four cases. To the contrary, the (h/v) spectral ratios of the experimental data show generally a 2 to 4 times lower amplitude than the corresponding synthetic ones. The lack of scattered waves in the synthetics and the fact that the amplitude of the (h/v) ratio is systematically lower in the observed data are evidence of a preferably enriched vertical component in the scattered wave field. The spectral ratio amplitudes of synthetic and observed data for both horizontal components are almost comparable for all frequencies examined. The (h/v) ratio amplitudes of the observed data for both horizontal components are also comparable, but that of the synthetics varies significantly.

In order to examine the influence of source properties on the (h/v) ratio, some parametric investigations were carried out. For this purpose, only one recording, the number 5 event (M_L = 4.2, R = 16 km) was considered. Starting with a constant fault direction, strike = 135°, that is close to the one of the San Jacinto fault, the following pairs of dip and rake were tested: (1) dip = 90°, rake = 0° (pure strike-slip fault), (2) dip = 45°, rake = 90°, and (3) dip = 45°, rake = 45° (reverse faults). As shown in Figure 15, the shape of the (h/v) ratio remains stable for both horizontal components in all three cases. To the contrary, the amplitudes of this ratio are dependent on the aforementioned parameters of the focal mechanism. In case (2), the observed deviation in amplitude between the two horizontal components is mainly due to the adopted radiation pattern of body waves. Tests done with different source-time function characteristics

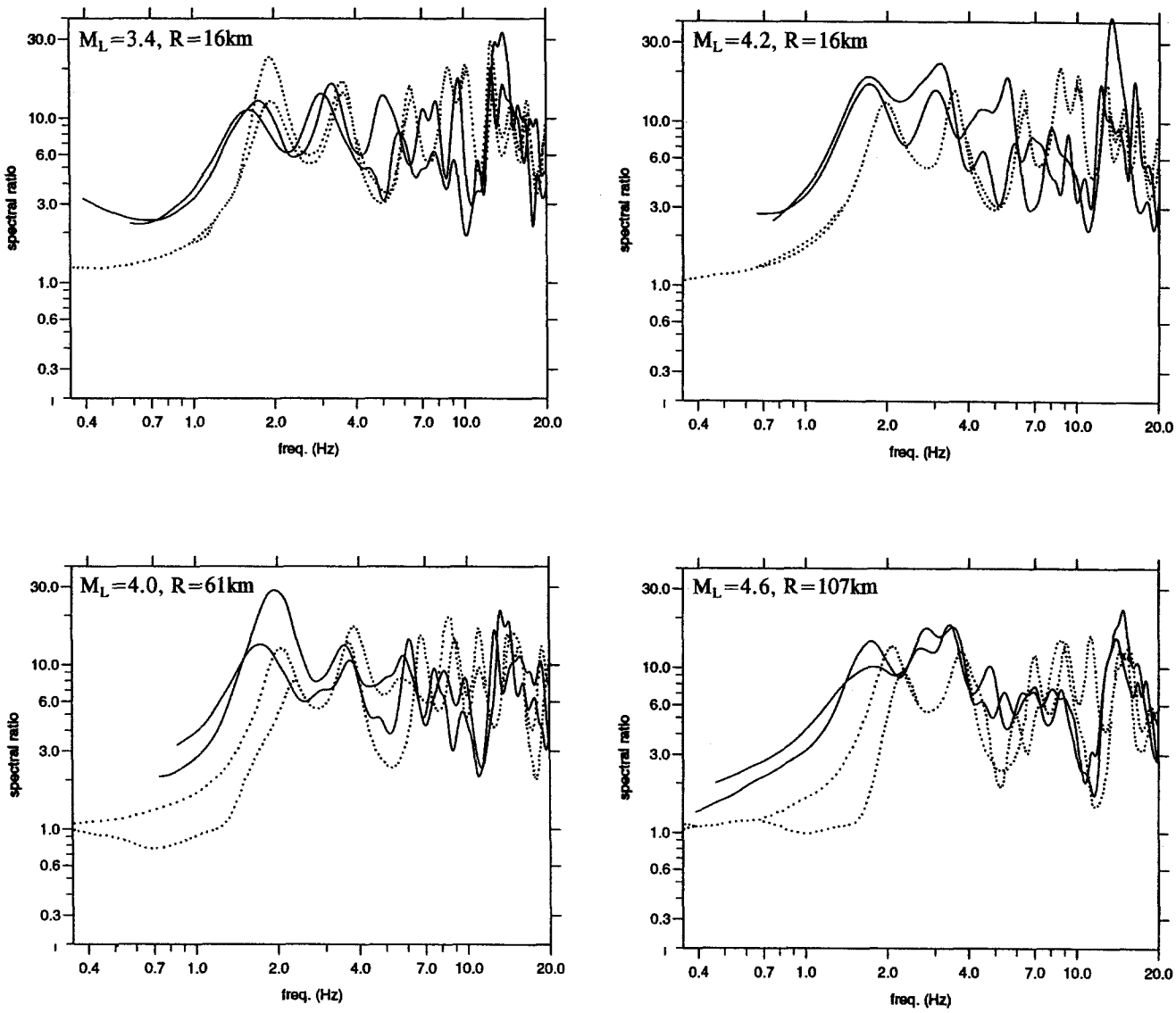

Figure 14. Spectral ratio (solid line) on the surface of GVDA for four selected recordings (Table 1, numbers 5, 7, 8, and 12), in comparison with those corresponding to the synthetic accelerograms generated by the discrete wavenumber method (dotted line).

showed, as expected, that the shape as well as the amplitude of the (h/v) ratio are not affected. Also, the absolute value of the seismic moment has no influence on the (h/v) ratio and on the spectral ratio.

Discussion and Conclusions

In this study, we have chosen a data set of accelerograms obtained at the Garner Valley surface and downhole array in southern California. We have selected events with the highest peak accelerations occurring during the first year of recording. The local magnitude of the events lies between 3.0 and 4.6, and the epicentral range extends from 6 to over 100 km. A signal-to-noise threshold equal to or greater than 3 was applied for each component before any further calculations.

A good stability of the (h/v) ratio is implied by the relatively low standard deviation values obtained on the surface and in all four different depths. The peaks of the (h/v) ratio appear clearly at 1.8, 6, and 8 Hz while less clearly at 3 and 13 Hz. The peak around 2 Hz is in agreement with the *S*-wave theoretical transfer function. The most prominent difference between the (h/v) ratio and the spectral ratio is in their absolute levels, with the latter being 2 to about 6 times higher.

The amplitudes of the (h/v) ratio, based on synthetic accelerograms generated by the discrete wavenumber method, are in satisfactory agreement with those of the spectral ratio technique. The systematically observed lower am-

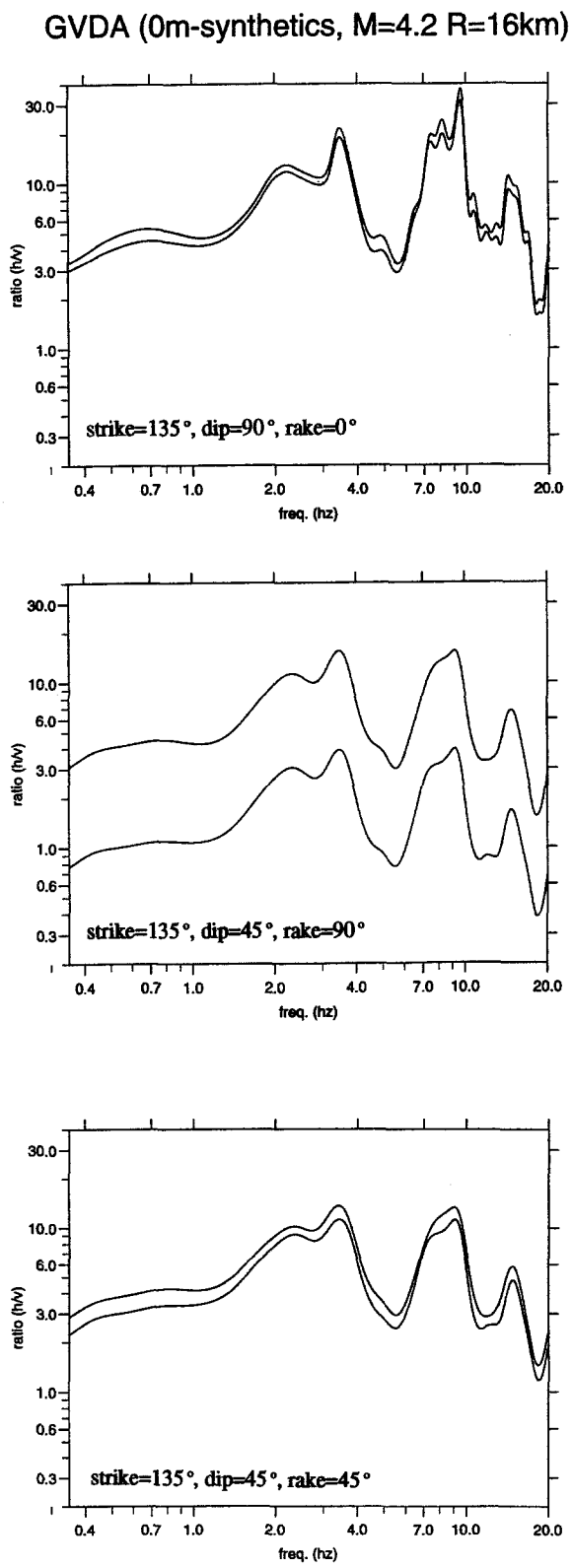

Figure 15. Influence of different source mechanisms on the (h/v) ratio for the same event generated by the discrete wavenumber method. The two curves in each plot refer to two horizontal components.

plitude of the (h/v) ratio, based on recorded accelerograms, is probably due, among other factors, to a relative enrichment of the vertical component of the scattered wave field, which is also evident in the comparison between the actual and the synthetic accelerograms (Fig. 12). In the latter, scattered waves are not simulated. However, the remarkable difference in amplitude between the observed (h/v) ratio and spectral ratio is a point that needs further research.

Source properties do not seem to affect the shape of (h/v) ratio, but they do influence its absolute level. As has been shown (Fig. 15), the focal mechanism radiation pattern does seriously affect the theoretical (h/v) ratio amplitude. Parametric investigation of the influence of the quality factor *Qp*, *Qs*, by increasing their values for the layers deeper than 22 m, showed that both shape and amplitude of the (h/v) ratio remain unchanged.

Acknowledgments

This research was supported in part by the Institut de Protection et de Surete Nucleaire of the Commissariat a l'Energie Atomique and in part by the EC projects (1) Volvi-Thessaloniki EUROSEISTEST (EV:5V.CT930281, DIR 12 SOLS) and (2) ERB4001GT921713. We thank Bagher Mohammadioun and Jean-Christophe Gariel for scientific discussions as well as Martin Chapman and two anonymous reviewers for their fruitful comments and suggestions.

References

Aki, K. (1988). Local site effects on strong ground motion, *Proc. Earthquake Engineering and Soil Dynamics II GT Div/ASCE,* Park City, Utah, 103–155.

Aki, K. (1993). Local site effects on weak and strong ground motion, *Tectonophysics* **218,** 93–111.

Archuleta, R., S. Seale, P. Sangas, L. Baker, and S. Swain (1992). Garner Valley downhole array of accelerometers: instrumentation and preliminary data analysis, *Bull. Seism. Soc. Am.* **82,** 1592–1621.

Archuleta, R., S. Seale, P. Sangas, L. Baker, and S. Swain (1993). Erratum, *Bull. Seism. Soc. Am.* **83,** 2039.

Aster, R. and P. Shearer (1991). High-frequency, borehole seismograms recorded in the San Jacinto fault zone, southern California. Part 2: Attenuation and site effects, *Bull. Seism. Soc. Am.* **81,** 1081–1100.

Bakun, W. and A. Lindh (1977). Local magnitudes, seismic moments, and coda durations for earthquakes near Oroville, California, *Bull. Seism. Soc. Am.* **67,** 615–629.

Blakeslee, S. and P. Malin (1991). High-frequency site effects at two Parkfield downhole and surface stations, *Bull. Seism. Soc. Am.* **81,** 332–345.

Bouchon, M. (1981). A simple method to calculate Green's functions for elastic layered media, *Bull. Seism. Soc. Am.* **71,** 959–971.

Coutant, O. (1989). Programme de simulation numerique AXITRA, *Rapport LGIT,* 1989.

Coutant, O. (1995). Observation of shallow anisotropy on local earthquake records at the Garner Valley Downhole Array, *Bull. Seism. Soc. Am.* (in press).

Duval, A.-M. (1994). Determination de la reponse d'un site aux seismes a l'aide du bruit de fond: evaluation experimentale, *Ph.D. Thesis,* Unin. Pierre et Marie Curie-Paris, 6.

Field, E. (1994). Earthquake site response estimation, *Ph.D. Thesis,* Columbia University, New York.

Field, E. and K. Jacob (1993). The theoretical response of sedimentary layers to ambient seismic noise, *Geophys. Res. Lett.* **20,** 2925–2928.

Field, E., A. Clement, K. Jacob, V. Aharonian, and P. Friberg (1993). Earthquake site response study in Giumri (formerly Leninakan), Armenia, using ambient noise observations, *Proc. Inter. Conf. on Continental Collision Zone Earthquake and Seismic Hazard Reduction,* Yerevan, Armenia (in press).

Finn, L. (1991). Geotechnical engineering aspects of microzonation, *Proc. 4th Int. Conf. on Seismic Zonation,* Stanford University, Stanford, California, 199–259.

Gariel, J.-C., B. Mohammadioun, and G. Mohammadioun (1993). L'experimentation sismique de Garner Valley: resultats preliminaires, *Proc. 3eme Colloque National AFPS,* Saint-Remy-les-Chevreuse, France.

Hauksson, E., T.-L. Teng, and T. Henyey (1987). Results from a 1500 m deep, three-level downhole seismometer array: site response, low Q values, and f_{max}, *Bull. Seism. Soc. Am.* **77,** 1883–1904.

Hough, S. and J. Anderson (1988). High-frequency spectra observed at Anza, California: implications for Q structure, *Bull. Seism. Soc. Am.* **78,** 692–707.

Joyner, W., R. Warrick, and A. Oliver (1976). Analysis of seismograms from a downhole array in sediments near San Francisco Bay, *Bull. Seism. Soc. Am.* **66,** 937–958.

Kennett, B. L. and N. J. Kerry (1979). Seismic waves in stratified half space, *Geophys. J. R. Astron. Soc.* **57,** 557–583.

Langston, C. A. (1979). Structure under Mount Rainier, Washington, inferred from teleseismic body waves, *J. Geoph. Res.,* **84,** B9, 4749–4762.

Lachet, C. and P.-Y. Bard (1994). Numerical and theoretical investigations on the possibilities and limitations of the "Nakamura's" technique, *J. Phys. Earth* **42,** 377–397.

Lermo, J. and J. Chavez-Garcia (1993). Site effect evaluation using spectral ratios with only one station, *Bull. Seism. Soc. Am.* **83,** 1574–1594.

Liu, H.-P., R. Warrick, R. Westerlund, E. Sembera, and L. Wennerberg (1992). Observation of local site effects at a downhole-and-surface station in the Marina district of San Francisco, *Bull. Seism. Soc. Am.* **82,** 1563–1591.

Malin, P., R. Waller, R. Borcherdt, E. Cranswick, E. Jensen, and N. Van Schaack (1988). Vertical seismic profiling of Oroville microearthquakes: velocity spectra and particle motion as a function of depth, *Bull. Seism. Soc. Am.* **78,** 410–420.

Mohammadioun, B., G. Mohammadioun, and J.-C. Gariel (1992). Preliminary results from a vertical array in Garner Valley, California, *Proc. 10th World Conference on Earthquake Engineering,* 1025–1030.

Nakamura, Y. (1989). A method for dynamic characteristics estimation of subsurface using microtremor on the ground surface, *QR RTRI* **30,** 25–33.

Ocmachi, T., Y. Nakamura, and T. Toshinawa (1991). Ground motion characteristics in the San Francisco Bay area detected by microtremor measurements, *Proc. 2nd Int. Conf. on Recent Advances in Geotechnical Earthquake Engineering and Soil Dynamics,* St. Louis, Missouri, 1643–1648.

Pecker, A. and B. Mohammadioun (1993). Garner Valley: analyse statistique de 218 enregistrements sismiques, *Proc. 3eme Colloque National AFPS,* Saint-Remy-les-Chevreuse, France.

Redpath, B. and R. Lee (1986). In-situ measurements of shear-wave attenuation at a strong motion recording site (abstract), *Earthquake Notes* **57,** 8.

Seale, S. and R. Archuleta (1989). Site amplification and attenuation of strong ground motion, *Bull. Seism. Soc. Am.* **79,** 1673–1696.

Seed, H. and I. Idriss (1970). Analysis of ground motions at Union Bay, Seattle, during earthquakes and distant nuclear blasts, *Bull. Seism. Soc. Am.* **60,** 125–136.

Shearer, P. and J. Orcutt (1987). Surface and near surface effects on seismic waves—Theory and borehole seismometer results, *Bull. Seism. Soc. Am.* **77,** 1168–1196.

Theodulidis, N. and P.-Y. Bard (1995). Horizontal to vertical spectral ratio and geological conditions: an analysis of strong motion data from Greece and Taiwan (SMART-1), *Soil Dyn. Earthquake Eng* **14,** 177–197.

Tucker, B. and J. King (1984). Dependence of sediment-filled valley response on input amplitude and valley properties, *Bull. Seism. Soc. Am.* **74,** 153–165.

Tucker, B., J. King, D. Hatzfeld, and I. Nersesov (1984). Observation of hard-rock site effects, *Bull. Seism. Soc. Am.* **74,** 121–136.

Institute of Engineering Seismology and Earthquake Engineering
Hapsa 1
GR-54626 Thessaloniki, Greece
(N.T.)

Laboratoire Central des Ponts-et-Chaussées
58 Bd. Lefebvre
75732 Paris Cedex 15, France
(P.-Y.B.)

Laboratoire de Géophysique Interne et Tectonophysique
Observatoire de Grenoble
UMR CNRS C5559
IRIGM, BP 53 X
38041 Grenoble Cedex, France
(P.-Y.B., M.B.)

Department of Geological Sciences and Institute for Crustal Studies
University of California at Santa Barbara
Santa Barbara, CA 93106
(R.A.)

Manuscript received 4 March 1995.